C. R. Physique 13 (2012) 227–236

Contents lists available at SciVerse ScienceDirect

Comptes Rendus Physique

www.sciencedirect.com

Use of large scale facilities for research in metallurgy

# X-ray coherent scattering in metal physics

## *Diffraction cohérente des rayons X en physique du métal*

Frédéric Livet [a,*], Mark Sutton [b]

[a] *SIMaP, Grenoble-INP, CNRS, UJF, BP 75, 38402 Saint Martin D'Hères, France*
[b] *Physics Department, McGill University, Montreal, Québec H3A 2T8, Canada*

ARTICLE INFO

*Article history:*
Available online 28 January 2012

*Keywords:*
Coherent scattering
Speckles
X-ray photon correlation spectroscopy
Fluctuation dynamics

*Mots-clés :*
Diffraction cohérente
Spectroscopie de correlation des photons X
Dynamique des fluctuations

ABSTRACT

In a coherent x-ray scattering experiment, interference of the waves diffracted across the sample is observed. This gives a speckle pattern in the observed scattering intensity, whereas a standard experiment leads to diffuse intensity or to broadening of a Bragg peak. Speckles correspond to the disorder configuration of the irradiated volume and their dynamics provide microscopic information of the time evolution of the sample microstructure.
After a brief description of the techniques used for the observation of speckles in an x-ray experiment, some examples of measured time dynamics are given. These concern reversible fluctuations and irreversible decomposition of unmixing or ordering alloys. A few experiments in defect imaging are described and the studies opened by free electron lasers are briefly discussed.


RÉSUMÉ

En conditions de diffraction cohérente des rayons X, on observe les interférences entre les ondes diffractées par l'échantillon. Cela conduit à l'observation de tavelures là où une expérience classique donne une intensité diffuse ou une raie de Bragg élargie. Les tavelures correspondent à la configuration locale du désordre dans le volume irradié.
Dans cet article, après une brève description des techniques mises en oeuvre pour observer des tavelures dans une expérience de rayons X, quelques exemples d'observation de leur dynamique temporelle sont donnés. On discutera d'abord le cas de fluctuations réversibles et ensuite de l'utilisation de cette technique pour étudier la dynamique irréversible de la décomposition d'alliages à démixtion ou à mise en ordre. On décrira quelque sepériences d'imagerie des défauts et on discutera des voies ouvertes par l'apparition des lasers à électrons libres.


## 1. Introduction

Microstructure has an overriding influence on the physical properties of metals. Many of the recent advances in materials processing consist of sophisticated treatments designed to control and modify this microstructure. The very fact that the

* Corresponding author.
*E-mail address:* frederic.livet@simap.grenoble-inp.fr (F. Livet).

1631-0705/$ – see front matter 
doi:10.1016/j.crhy.2011.11.009

properties of materials depend on its processing history indicate that microstructure is a non-equilibrium phenomenon. Diffraction, in particular with x-rays, provides a direct probe of microstructure. In the last several years, new synchrotron sources (SRS) have been shown to have sufficient coherent x-ray flux to perform time-resolved diffraction experiments. These measurements are leading to new insights into the structure and dynamics of microstructure.

In a diffraction experiment, one observes the interference of scattered waves from a small 3-dimensional volume, called the coherence volume. For typical x-ray experiments, this volume has dimensions less than a micron and the measured intensity corresponds to a sum of the contributions from a large number of coherence volumes. In this case, the local configuration of each coherence volume cannot be determined, and the experiment measures an average of the sample properties over the irradiated volume. By limiting the diffraction volume to the coherence volume, extra information about the structure is available. In a simplified image, this can be described as the observation of the Fourier transform of the sample configuration. The Fourier intensity has strong fringes, irregular if resulting of summing a set of random amplitudes, called "speckles". That is of course, provided one has enough diffracted intensity.

The coherence volume can be split into a transverse $\Lambda_t$ and longitudinal $\Lambda_l$ (or temporal) coherence. $\Lambda_t$ is connected to the beam divergence $\epsilon$. A rough approximation, valid for slit limited beams gives [1]:

$$\epsilon \times \Lambda_t \simeq \lambda/2 \tag{1}$$

For x-rays with $\lambda \simeq 1.5$ Å and $\epsilon \simeq 10$ µrad $\Lambda_t$ is 10 µm. For an SRS of size $\sim 500$ µm at a 50 m distance, $\epsilon \sim 10$ µrad. With focusing optics, $\epsilon$ can be selected by upstream slits.

$\Lambda_l$ is directly related to the beam monochromaticity (with $\delta\lambda/\lambda$ the relative bandwidth):

$$\Lambda_l \simeq \lambda^2/(2 \cdot \delta\lambda) \tag{2}$$

where $\delta\lambda/\lambda$ is the relative bandwidth, which yields $\Lambda_l$ of the order of 0.5 µm with a Si(111) monochromator.

SRS now provides beams of high intensities in this angular range and this opens the possibility of carrying out experiments with fully (or at least partially) coherently irradiated samples [2]. A simple expression connects the coherent intensity available $I_c$ to the SRS brilliance $\mathcal{B}$:

$$I_c = \mathcal{B}\,(\lambda/2)^2(\delta\lambda/\lambda) \tag{3}$$

For an undulator beamline at third generation sources (APS, ESRF, Spring 8, Soleil, Petra III, Diamond, SLS, …), $\mathcal{B} \sim 10^{20}$ ph/(mrad$^2$ mm$^2$ s) for a 0.1% bandwidth. This gives an estimate of $I_c \sim 10^{11}$ ph/s with a Si(111) monochromator at $\lambda = 1.5$ Å. In practice, $I_c \simeq 10^{10}$ ph/s, but coherent experiments can be carried out with as little as $I_c \simeq 10^6$ ph/s.

In this article, we will focus on the observation of speckles in x-ray experiments. Studies of the dynamics of fluctuations in metals and alloys will be described. A special emphasis will be given on studies of irreversibility in phase transitions. The rapidly growing domain of lens less imaging which also emphasizes coherence is out of the scope of this paper, but some experiments of the observation of single crystal defects will be mentioned. The possibilities for surface studies is briefly explained. The new possibilities with the emergence of new SRS and of free electron laser sources (FEL), which supply an essentially fully coherent source are discussed.

## 2. Observation of speckles

In a coherent experiment, the irradiated volume is of the order of the coherence volume. For transverse coherence, this is achieved either by studying small samples (from a few µm to a few nm) or by limiting the transverse beam size by slits or pinholes of diameter $\phi \approx \Lambda_t$. Longitudinal coherence limits the size of the irradiated region by the condition that path length differences across the irradiated sample $\Delta\mathcal{L}$ remain of the order of $\Lambda_l$.

### 2.1. Detection

The interference pattern which defines the speckles, gives them a typical angular size comparable to the beam divergence. Thus for the observation of speckles, a high resolution detector is needed having an angular aperture $\epsilon'$ on the order of the beam divergence $\epsilon$. For 10 µrd, a 20 µm aperture at 2 m suffices. In this small solid angle, the detected intensity may be low and the use of area detectors is highly beneficial. A pixel size of 20 µm is standard for a CCD chip and direct illumination CCDs are frequently used in these experiments [3]. These CCDs have relatively low readout frequencies (less than a few MHz) and their characteristics slightly degrade with radiation exposure. Recently, "pixel array detectors" were developed of 55 µm resolution [4], with very high counting rates [5]. Their lower resolution can be compensated by the smaller beam sizes ($\phi \sim 1$ µm) now commonly available with the progress in x-ray optics or by increasing the sample to detector distance over 10 m.

### 2.2. Speckles in small angle x-ray scattering

In material science problems, small angle scattering (SAXS in the case of x-rays) gives important information on the size of inclusions which contribute to sample strengthening. A classical example is the Al–Li binary alloy, where $Al_3Li$ ordered

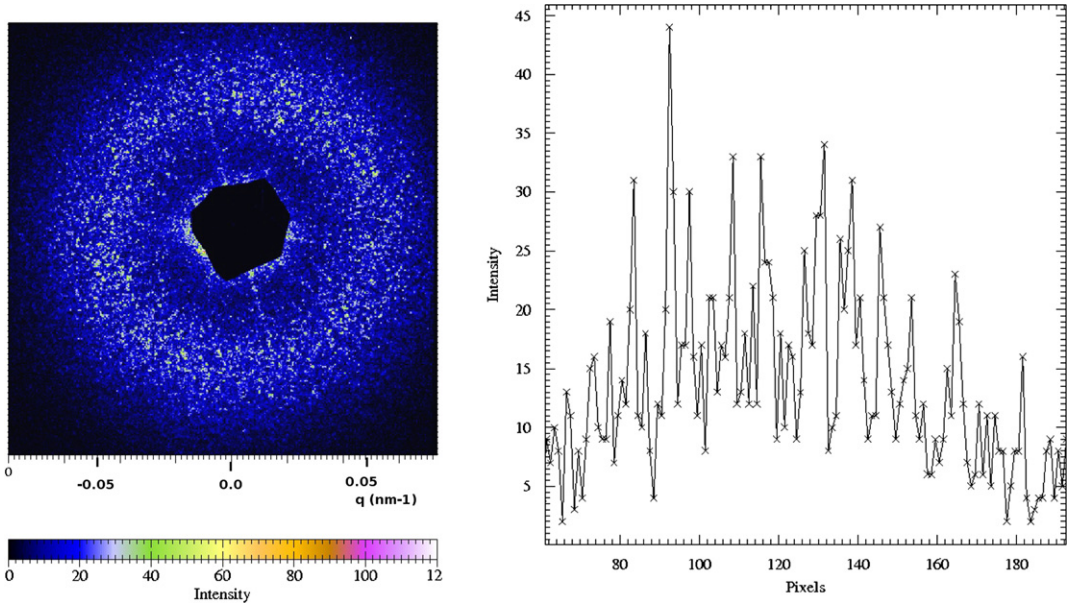


**Fig. 1.** SAXS observation of a speckle structure in the diffraction ring of an Al–Li decomposed alloy. The units of intensity are x-ray counts. The crystal has a (110) orientation along the beam, the radius of the $Al_3Li$ spherical precipitates is roughly 50 nm and the figure shows a $0.16 \times 0.16$ nm$^{-1}$ region of the reciprocal lattice. The central black region is the shadow of a beam stop to prevent the main beam from hitting the detector. The right figure shows a typical profile observed across one side of the ring.

spherical precipitates can be observed in a conventional SAXS experiment [6]. In Fig. 1, typical coherent SAXS scattering is shown. This figure was obtained at the D2AM bending magnet beamline of ESRF with a 22 µm resolution CCD detector at 2.2 m downstream the sample [7]. The detector was used in a photon counting mode, providing high quality measurements for low counting rates [3]. The intensity profile shown at the right side of Fig. 1 shows the intensity fluctuations due to speckle observed along a line crossing the ring created by spherical interfering particles.

In the experiment of Fig. 1, an $e \simeq 0.1$ mm thick sample could be studied in a reasonable angular domain by closing slits in order to select a transversely coherent beam of size $\phi \simeq 10$ µm. In a SAXS experiment, with a transmission geometry, two terms contribute to $\Delta\mathcal{L}$:

$$\Delta\mathcal{L} = 2 \cdot \phi \times \theta \tag{4}$$

and

$$\Delta\mathcal{L} = 2 \cdot e \times \theta^2 \tag{5}$$

In SAXS, with a Si(111) monochromator, $\Delta\mathcal{L}$ is significantly smaller than $\Lambda_l$, and experiments can even be carried out by using the 1% bandwidth "pink beam" obtained by filtering a harmonic of an undulator [8–10].

When the coherence volume is smaller than the diffraction volume the beam is said to be partially coherent. Such beams have reduced fluctuations in their speckles. An incoherent beam can be considered as the result of such a large diffraction volume that the speckle contrast cannot be observed. Speckle contrast $\beta$ can be estimated from the variations of the intensity, as compared to an incoherent SAXS intensity $S(\vec{q})$. For isotropic scattering

$$1 + \beta(q) = \frac{\langle I(q)^2 \rangle - S(q)^2}{S(q)^2} \tag{6}$$

In this equation, the "1" arises because of Poisson noise and the averages are over regions with the same magnitude, $|\vec{(}q)|$. This means that $S(\vec{q})$ has to be measured under equivalent conditions. In practice, the angular average in the experiment of Fig. 1 provides an estimate of $S(\vec{q})$: $S(q) = \langle I(\vec{q}) \rangle_{|\vec{q}|=q}$, assuming that this intensity is isotropic. A value $\beta \simeq 0.2$ was obtained from Eq. (6), independent of $|\vec{q}|$. It is a mean square deviation, and the speckle variations of the intensity are of the order of 50% (see right side curve of Fig. 1). In some papers, the speckle "visibility" is defined, as $\sqrt{\beta}$. These speckles correspond to averaging over $1/\beta \simeq 5$ coherence volumes. In speckle experiments, improving coherence lowers significantly the available intensity, and optimizing the setup may significantly improve the signal to noise ratio [1]. For pink beam experiments, $\Lambda_l \simeq 7$ nm, and, from Eqs. (4) and (5), the contrast rapidly decreases with $\theta$.

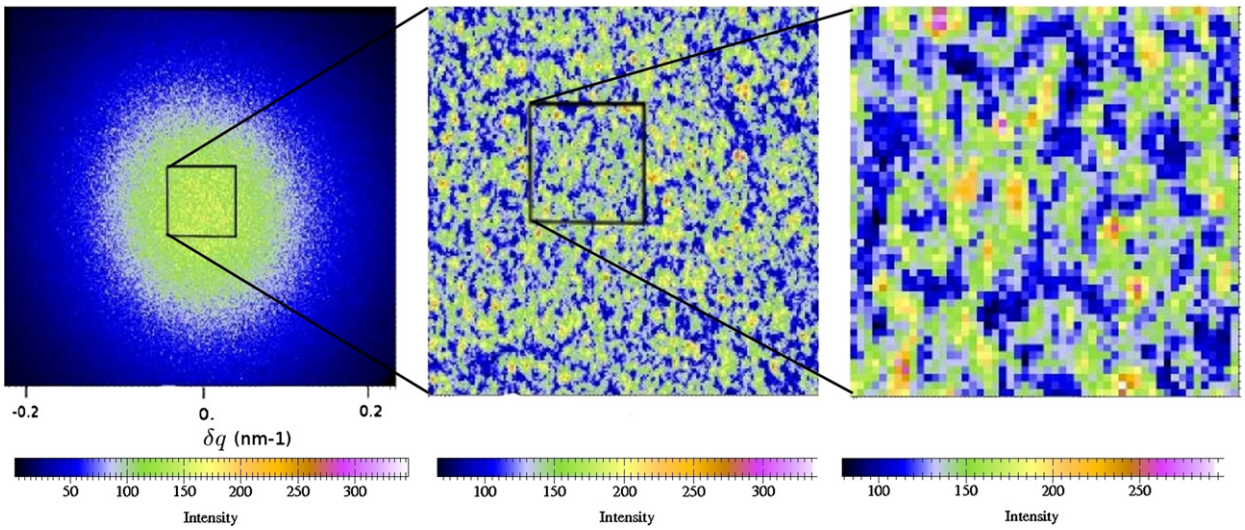


**Fig. 2.** Image of the (001) superstructure peak from a Cu–Pd $L1_2$ ordering alloy. $\delta q$ (in $nm^{-1}$ units) is the distance from the superstructure peak position in the reciprocal lattice. Enlarged figures from each selection square are drawn at the right side in order to show the numerous speckles.

### *2.3. Speckles at large angle*

In the vicinity of a Bragg peak, at large $\theta$, the condition implied by Eq. (5) is satisfied only if the longitudinal dimension of the diffracting volume is a few microns. This can be achieved for thin enough samples or by studying strongly absorbing samples in the Bragg reflection geometry. If the absorption length is $\mu^{-1}$, one writes:

$$\Delta\mathcal{L} = 2 \times \mu^{-1} \sin^2\theta \tag{7}$$

An example is given by the superlattice peak of the Cu–Pd ordering alloy [11]. In this alloy, the $L1_2$ ordered structure induces a (001) superstructure peak. The ordering dynamics is slow, and in a conventional diffraction experiment, the (001) peaks are broadened by the presence of numerous antiphase domains. In a coherent scattering experiment, this superlattice peak exhibits speckles as shown in Fig. 2.

In Fig. 2, incoherent scattering is slowing varying as the domains coarsen. An estimate of $\beta \simeq 0.044$ can be obtained from Eq. (6) by studying the speckle variations of a single image (see Fig. 2). Here, $\Delta\mathcal{L} \simeq 1$ µm from Eq. (7), which is significantly larger than $\Lambda_l \simeq 0.5$ µm, and this reduces $\beta$ from 0.25, as measured in a SAXS configuration to 0.044.

## 3. Reversible fluctuations: Phasons

For stationary processes, the dynamics of microscopic fluctuations can be observed. From measurements of the fluctuations of the time-dependent intensity $I(\vec{q},t)$, one can study the intensity–intensity correlations:

$$\gamma(\vec{q},t) = \frac{\langle I(\vec{q},t')I(\vec{q},t+t')\rangle_{t'}}{\langle I(\vec{q},t')\rangle_{t'}^2} \tag{8}$$

and $\gamma(\vec{q},t)$ can be expressed in the form [12]:

$$\gamma(\vec{q},t) = 1 + \beta(q)\, g^{(2)}(\vec{q},t) \tag{9}$$

For low intensity x-ray experiments, $g^{(2)}$ is calculated from a set of pixels of an area detector, and assumed isotropic:

$$1 + \beta(q)\, g^{(2)}(q,t) = \frac{\langle\langle I(\vec{q},t')\, I(\vec{q},t+t')\rangle_{t'}\rangle_{\vec{q}}}{\langle\langle I(\vec{q},t')\rangle_{t'}\rangle_{\vec{q}}^2} \tag{10}$$

This technique is called x-ray photon correlation spectroscopy (XPCS) [13,14], or x-ray intensity fluctuation spectroscopy (XIFS). It has been used for the study of phasons in *i*-AlP dMn quasicrystal [15]. In this system, phasons are modes introduced in a "perpendicular space", in a similar way as phonon modes. These modes have a diffuse scattering similar to that of phonons, but they are stable at room temperature and speckles could be observed in the diffuse scattering [16].

For temperatures higher than 600 °C, phason fluctuations are observed from changes in the speckle pattern. Fig. 3 shows the time evolution of the speckles observed at two different $q$-values in the vicinity of a quasicrystal Bragg reflection of low index (7/11 in N/M indices). The correlation function was fitted with an exponential:

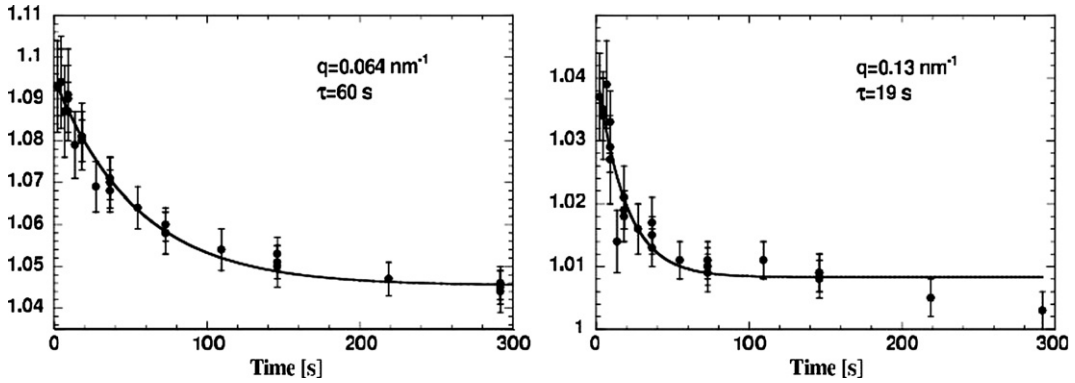


**Fig. 3.** Correlation function $1 + \beta g^{(2)}(q, t)$ observed at 650 °C for two different q-vectors.

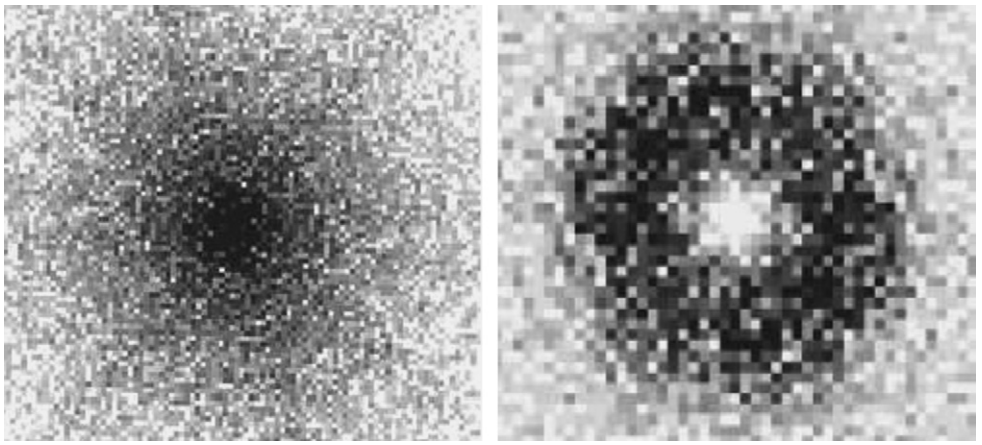

**Fig. 4.** Speckle patterns obtained from Monte Carlo simulations in model "A" (left) and model "B" (right). These images result from the modulus squared of the configuration Fourier transform, in order to simulate the coherent observed intensities.

$$g^{(2)}(q, t) = \exp\bigl(-2t/\tau(q)\bigr) \tag{11}$$

and $\tau(q) \propto q^{-2}$. At 650 °C, $\tau \simeq 60$ s for a 100 nm fluctuation length, and a temperature variation in rough agreement with a $3.0 \pm 1.0$ eV activation energy.

## 4. Phase transformations

### *4.1. Two models*

In materials, phase transitions (PT) are an important way of modifying mechanical properties and dynamical studies should provide insight into this way of controlling the microstructure. Two main models for PT dynamics can be distinguished [17] and they lead to different time dependence of the characteristic length scale $\mathcal{R}(t) \propto t^{1/n}$:

- Model "A", with $n = 2$, corresponding to an ordering system, where local order is changed by the exchange of two atoms between neighboring sites (non-conserved order parameter).
- Model "B", with $n = 3$, corresponding to unmixing, where atoms have to be transported across the sample (conserved order parameter).

These two universality classes can be related to Ising Hamiltonians, and simulations of the time-dependent configurations have been carried out [18,19]. From Fourier transforms of these configuration, typical speckle figures are obtained. Fig. 4 shows the results obtained with the two models.

The right part of Fig. 4 is obtained in a SAXS region (which can be called the (000) Bragg peak) and it shows a ring similar to the one observed in Fig. 1 characteristic of unmixing system. The left part is obtained in the vicinity of an ordering Bragg peak, and can be compared with Fig. 2, an ordering system. These figures correspond to times where two well identified phases with well defined interfaces have developed.

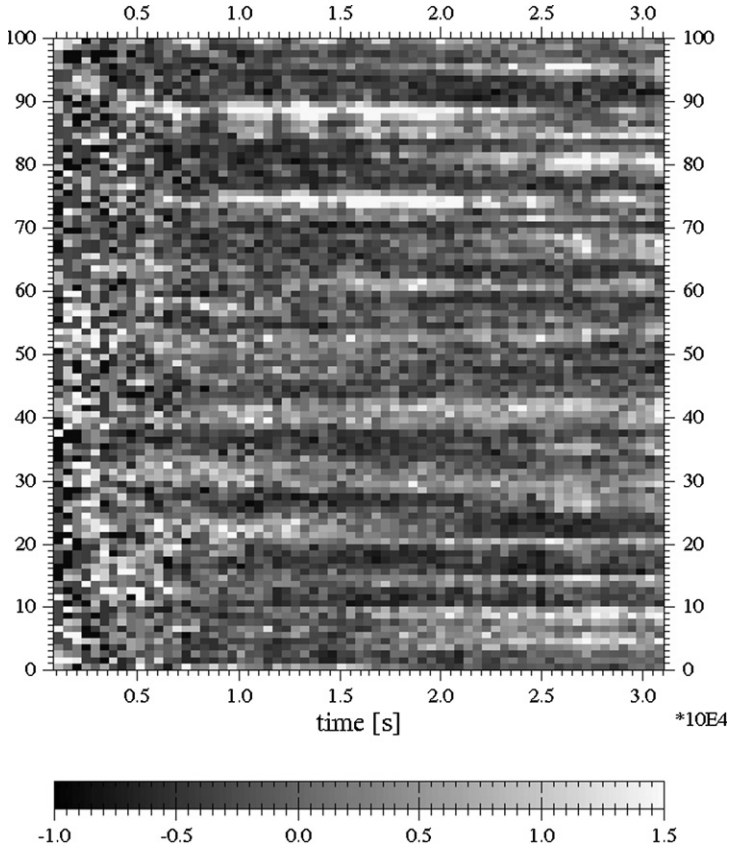


**Fig. 5.** Time evolution of the normalized speckle intensity for a set of pixels with the same $|\vec{q}| \simeq 0.117$ nm$^{-1}$ value. The Al–Li$_{9\%}$ single crystal is aged at 220 °C.

### *4.2. Irreversibility*

In the dynamic study of PT, the stochastic processes are not stationary (or ergodic), and Eq. (8) cannot be used. The incoherent intensity in both cases varies in time. Since the incoherent intensity is expected to satisfy dynamical scaling:

$$S(\vec{q},t) = \mathcal{R}(t)^3 \times \Phi\big(q\mathcal{R}(t)\big) \propto t^{3/n} \times \Phi'\big(qt^{1/n}\big) \tag{12}$$

This equation holds for a 3d system, and the scaling functions (neglecting anisotropy) $\Phi(x)$ and $\Phi'(x)$, have different shapes between models A and B (as in both sides of Fig. 4). For coherent experiments, one can obtain $S(\vec{q},t)$ by averaging or smoothing away the speckles:

$$S(\vec{q},t) = \big\langle I(\vec{q},t\big\rangle_{\vec{q}} \tag{13}$$

The dynamics of speckles in these systems can be obtained from the study of the intensity variations versus the time-dependent mean $S(\vec{q},t)$:

$$D(\vec{q},t) = I(\vec{q},t)/\big\langle S(\vec{q},t)\big\rangle_{\vec{q}} - 1 \tag{14}$$

In Al–Li (Fig. 1), the scattering can be assumed isotropic and angular averages can be used. For Cu–Pd, where the scattering is anisotropy, a careful Gaussian smoothing of the time-dependent intensity had to be carried out.

Fig. 5 shows the typical time variations of $D(\vec{q},t)$ for various pixels at the same $|\vec{q}|$-value. This normalized intensity exhibits fast variations for short times after quench and a persistent speckle configuration in the long term.

### *4.3. Correlations during Al–Li coarsening*

In all systems studied, this speckle pattern persistence was observed. This will be discussed in some detail for the experiment on the unmixing of the Al–Li alloy. The sample was quenched from 475 °C to 220 °C and then its coherent SAXS was measured for about 8 hours. In this system and at this temperature, the Ostwald ripening quasi-stationary process is observed after a few seconds. The $n = 3$ behavior, typical of model B process is observed for a long time range. Classically

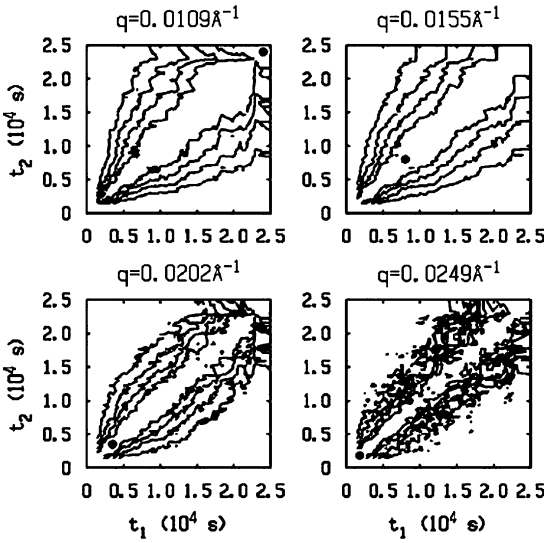


**Fig. 6.** Contours of the $C_{norm}(q, t_1, t_2)$ obtained with the Al–Li alloy. The speckle time variations are faster for larger $q$-values. A black dot indicates the time of maximum intensity $t_{\max}$ for each given $q$.

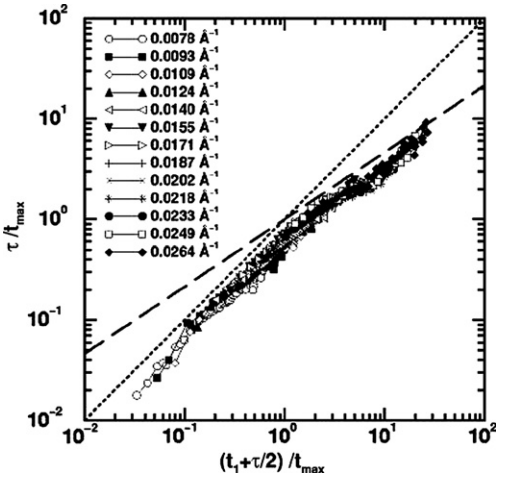


**Fig. 7.** The ratio $\tau/t_{\max}$ is compared to the ratio of the aging time divided by $t_{\max}$. For large values of this ratio, the fluctuation time losses its linear dependence. This may indicate surface fluctuation of large precipitates.

for a given $q$-value, the intensity initially increases, reaches a maximum $t_{\max}$ and then slowly decreases (see Fig. 3 in [20]). The time $t_{\max}$ can be used to scale all times.

The time correlations can be studied using the two-time correlation function:

$$C(q, t_1, t_2) = \left\langle D(\vec{q}, t_1)\ D(\vec{q}, t_1) \right\rangle_{\vec{q}} \tag{15}$$

$C(q, t_1, t_2)$ can be normalized by dividing by $\beta$, and $C_{norm}(q, t_1, t_2)$ can be plotted. Fig. 6 shows typical results in Al–Li as contour plots.

An estimate of the correlation time $\tau$ is obtained from the shape of $C_{norm}(q, t_1, t_2)$ [20]. The scaled time $\tau/t_{\max}$ is compared to the scaled time after the quench ($t_Q/t_{\max} = (t_1 + t_2)/2t_{\max}$) in Fig. 7. This latter ratio is a normalized aging time. For short times, $\tau \simeq t_{\max}$, and for longer times ($t_Q/t_{\max} \gg 1$), a power law with exponent 2/3 has been plotted for comparison. In a simple model, the linear slope corresponds to a persistent of the initial spatial configuration of the spherical precipitates. For long times and short distances, the 2/3 behavior corresponds to surface fluctuations of large precipitates and is directly related to Porod's law. In Fig. 6, this region corresponds to $q = 0.0249$ Å$^{-1}$, where the contours become more parallel to the diagonal ($t_1 = t_2$), which means only a small increase of $\tau$ vs $(t_1 + t_2)/2$.

Dynamical scaling for both model "A" and model "B" predicts this initial linear time behavior followed by a late time $1 - 1/n$ power law [18,19]. Fluerasu et al. [21] present data for the non-conserved case, model "A".

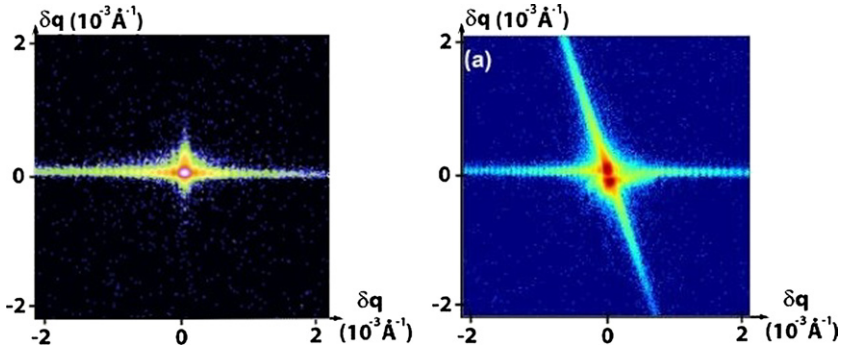


**Fig. 8.** Bragg diffraction of a perfect Silicon crystal (left) and of a crystal with a single dislocation in the middle of the irradiated area (right). The Bragg peak is doubled because of the phase shifts in the scattering from around the dislocation. The horizontal fringes are diffraction from the upstream slits and the streak close to the vertical direction is interpreted in connection with dislocation dissociation [28].

### *4.4. Stochastic process*

In the case of a slow transformation process, the statistical study of the time series of the coherent intensity can be carried out. This was used for the study of unmixing [22]. This needs to study the dimension $\alpha$ of the mean-square growth $F(q,t)^2$ of the measured intensities:

$$F^2(q,t) = \left\langle \left\langle \left( I(\vec{q},\tau) - I(\vec{q},t+\tau) \right)^2 \right\rangle_\tau \right\rangle_{\vec{q}=q} \propto t^{2\alpha} \tag{16}$$

The comparison of the $\alpha$ values obtained in two systems, Al–Ag and Al–Zn, was interpreted by two different coarsening mechanisms: the first system has a classical evaporation–condensation Lifschitz–Slyozov–Wagner (LSW) behavior and the second follows a coagulation process, where precipitates move and coalesce. This method was also applied to the study of the antiphase fluctuations, showing an anti-correlation movement [23].

## 5. The observation of defects

Coherent x-ray scattering opens a new imaging method called coherent diffraction imaging (CDI). In CDI, the goal is to obtain real space images of samples from the measured diffracted intensity. This requires developing algorithms to recover the phase of the diffracted amplitude. First developments were in the observation of nanoobjects [24,25], and scanning diffraction microscopy methods (ptychography) [26] open now the possibility of imaging large objects by scanning across the sample. A short review of the various techniques is given in [27].

In this case, a high quality measurement of the intensity diffracted by the sample is mandatory, and this requires that the irradiated sample volume is smaller than the coherence volume: $\beta \simeq 1$.

Apart from imaging, coherent scattering brings a high sensitivity to individual defects and coherent scattering provides a method for the study of samples with a single – or a small number of – defects(s).

For nearly perfect crystals, the occurrence of a single defect, like a dislocation, changes the scattering of a perfect crystal in a measurable way [29]. This was observed in a silicon single crystal with a single dislocation in the irradiated area [28]. In Fig. 8, a perfect crystal Bragg peak is shown (left): the fringes in the horizontal direction correspond to the diffraction by the crystal of the slit scattering. The right side of the figure shows the scattering observed at the (220) Bragg position with a single dislocation in the irradiated area. As the dislocation induces a phase shift in its vicinity, the Bragg peak is split due to destructive interference.

The observation of dislocation-like defects as sudden phase changes in charge density waves [30–32] or spin density waves [33] has been reported, and this suggests possible dynamical studies in response to a field disrupting the system.

## 6. Surface studies

In an x-ray experiment, the sample surface is the main defect for a high quality single crystal. In an incoherent x-ray scattering experiment, the corresponding diffraction leads to a crystal truncation rod (CTR) [34]. The longitudinal variations of the CTR (the $q_\parallel$ direction) intensity correspond to surface roughness and deformation, and the transverse width $\delta q_\perp$ to the inverse of the size of surface terraces. In a coherent experiment, a 2-dimension map of the intensity measured in the $\vec{q}_\perp$ plane corresponds to the Fourier transform of the surface configuration. At the "antibragg" (AB) position of the CTR, monoatomic step in surface can be studied. The extension of the speckles along the $q_\parallel$ is a proof that speckles in the $q_\parallel$ plane correspond to monoatomic steps. This could be done [35] on a $Si_{111}$ crystal in the vicinity of the $(\frac{1}{2}\frac{1}{2}\frac{1}{2})$ AB position (see Fig. 9). This brings a promising method for static and dynamical surface studies, as in a pioneering work of Pierce et al. [36].

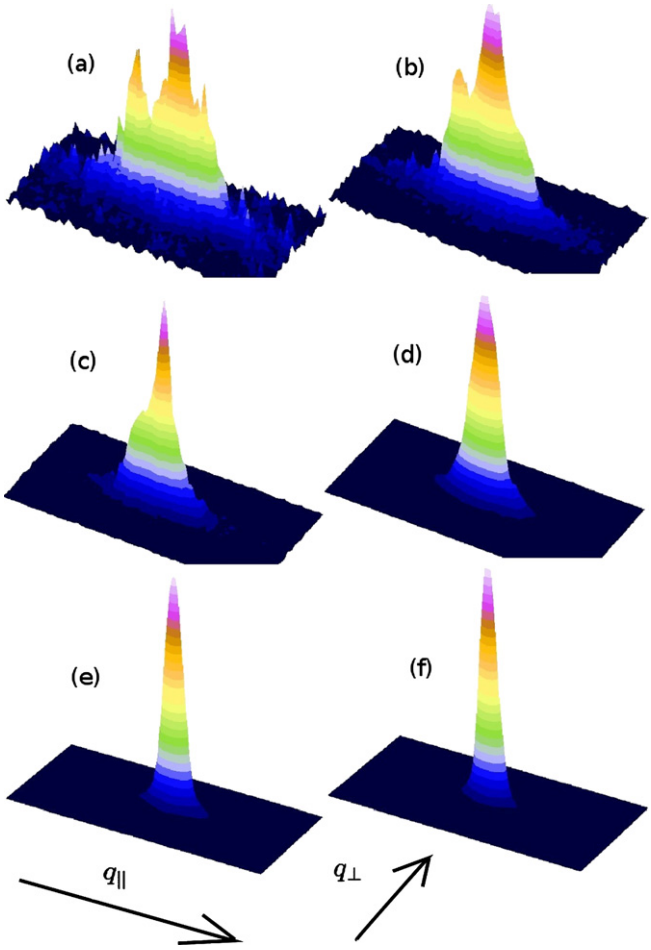


**Fig. 9.** The transverse shape of the truncation rod of a Si(111) single crystal for $(h, h, h)$ vectors: (a) $h = 0.5$, (b) $h = 0.56$, (c) $h = 0.63$, (d) $h = 0.69$, (e) $h = 0.75$, (f) $h = 0.81$ [35]. Intensities are in arbitrary linear units. The figures show the same number of detector pixels in the vicinity of the CTR. Close to the AB position, speckles are observed, corresponding to surface steps, and close to the Bragg position, a single peak shows a perfect crystal. One notices that the speckle extension is large in the $q_{\parallel}$ direction, indicating monoatomic steps.

Surfaces can be studied at AB positions in the case of high quality crystals, as for instance silicon. For metal samples, the coherent surface scattering cannot be observed if grain boundaries or even a small number of dislocations are in the irradiated area. As careful high temperature annealing of crystals is necessary for obtaining defect free regions of a few µm, studies will be developed for micron size beams now available with recent x-ray focusing optics.

## 7. Discussion

In all these experiments, the measured speckle intensity is highly connected to the number of atoms collectively contributing to the cross section and to the beam coherent intensity per unit area. For future experiments in material science, one can enumerate some desired improvements many of which are under way:

- micron or sub-micron size x-ray beams;
- improved source brilliance;
- improved high-quality crystalline samples;
- a larger $\Lambda_l$ from better energy resolution;
- better x-ray optics;
- improved x-ray detectors.

Just starting are new free electron laser (FEL) sources (LCLS, Stanford) which have large intensities and femtosecond pulses. FELs will give access to a new regime for time-resolved experiments. FELs provide a huge increase in beam power density, so much larger that the sudden burst of heat they create can destroy the sample. Still, it should be possible to perform single shot experiments, measuring the diffraction of the system before destruction or even during for the study the destruction processes itself. For some samples, it should be possible to use enough beam attenuation or extremely narrow

bandwidth selection to study them in less destructive mode. Other new SRS, like the energy recovery linacs proposed at Cornell [37,38], can potentially lead to more continuous like sources but with brilliance one or two orders of magnitude higher than SRS presently available.

These improvements, together with progress in preparing high quality crystal samples will make some currently difficult experiments possible. Obvious examples such as surface studies, where the number of surface atoms is small, and diffuse scattering experiments, which depend of the few atoms involved in the short-range fluctuations. With a FEL, dynamic studies of defects involving a small number of atoms or from the short-range order of liquids will be attainable.

## References

[1] F. Livet, Diffraction with a coherent x-ray beam: dynamics and imaging, Acta Crystallogr. A 63 (2007) 87–107.
[2] M. Sutton, S.G.J. Mochrie, T. Greytak, S.E. Nagler, L.E. Berman, G.E. Held, G.B. Stephenson, Observation of speckle by diffraction with coherent x-rays, Nature 352 (1991) 608–610.
[3] F. Livet, F. Bley, J. Mainville, M. Sutton, S. Mochrie, E. Geissler, G. Dolino, D. Abernathy, G. Grübel, Using direct illumination ccds as high-resolution area detectors for x-ray scattering, Nucl. Instr. Meth. A 451 (2000) 596–609.
[4] R. de Vries, S. Weijers, K. Bethke, V. Kogan, J. Vasterink, A. Kharchenko, M. Fransen, J. Bethke, Medipix 2 in x-ray diffraction, Nucl. Instr. Meth. A 576 (2007) 164–168.
[5] C. Ponchut, J. Clément, J.-M. Rigal, E. Papillon, J. Vallerga, D. LaMarra, B. Mikulec, Photon-counting x-ray imaging at kilohertz frame rates, Nucl. Instr. Meth. A 576 (2007) 109–112.
[6] F. Livet, D. Bloch, A kinetic analysis of Al–$Al_3Li$ unmixing, Scripta Met. 10 (1985) 1147.
[7] F. Livet, F. Bley, A. Létoublon, J.P. Simon, J.F. Bérar, Coherent small-angle scattering on a bending-magnet beamline at the ESRF, J. Synchr. Rad. 5 (1998) 1337–1345.
[8] D.L. Abernathy, G. Grübel, S. Brauer, I. McNulty, G.B. Stephenson, S.G.J. Mochrie, A.R. Sandy, N. Mulders, M. Sutton, Small angles x-ray scattering using coherent undulator radiation at the ESRF, J. Synchr. Rad. 5 (1998) 37–47.
[9] A. Malik, A.R. Sandy, L.B. Lurio, G.B. Stephenson, S.G.J. Mochrie, I. McNulty, M. Sutton, Coherent x-ray study of fluctuations during domain coarsening, Phys. Rev. Lett. 81 (1998) 5832–5835.
[10] E.M. Dufresne, T. Nurushev, R. Clarke, S.B. Dierker, Concentration fluctuations in the binary mixture hexane–nitrobenzene with static and dynamic x-ray scattering, Phys. Rev. E 65 (2002) 061507.
[11] K. Ludwig, F. Livet, F. Bley, J.P. Simon, R. Caudron, D.L. Bolloc'h, A. Moussaid, X-ray intensity fluctuation spectroscopy studies of ordering kinetics in a Cu–Pd alloy, Phys. Rev. 72 (2005) 144201.
[12] B.J. Berne, R. Pecora, Dynamic Light Scattering, Dover Publications, New York, 2000.
[13] S. Dierker, R. Pindak, R. Fleming, I. Robinson, L. Berman, X-ray photon correlation spectroscopy study of Brownian motion of gold colloids in glycerol, Phys. Rev. Lett. 75 (1995) 449.
[14] G. Grübel, F. Zontone, Correlation spectroscopy with coherent x-rays, J. Alloys Compounds 362 (2004) 3–11.
[15] S. Francoual, F. Livet, M. de Boissieu, F. Yakhou, F. Bley, A. Létoublon, R. Caudron, J. Gastaldi, Dynamics of phason fluctuations in the i-AlP dMn quasicrystal, Phys. Rev. Lett. 91 (2003) 225501.
[16] A. Létoublon, F. Yakhou, F. Livet, F. Bley, M. de Boissieu, L. Mancini, C. Vettier, J. Gastaldii, Coherent x-ray diffraction and phason fluctuations in quasicrystals, Europhys. Lett. 54 (2001) 753–759.
[17] P.C. Hohenberg, B.I. Halperin, Theory of dynamic critical phenomena, Rev. Mod. Phys. 49 (1977) 436–479.
[18] G. Brown, P.A. Rikvold, M. Sutton, M. Grant, Speckle from phase-ordering systems, Phys. Rev. E 65 (1997) 6601–6612.
[19] G. Brown, P.A. Rikvold, M. Sutton, M. Grant, Evolution of speckle during spinodal decomposition, Phys. Rev. E 60 (1999) 5151–5162.
[20] F. Livet, F. Bley, R. Caudron, E. Geissler, D. Abernathy, C. Detlefs, G. Grübel, M. Sutton, Kinetic evolution of unmixing in an AlLi alloy using x-ray intensity fluctuation spectroscopy, Phys. Rev. E 63 (2001) 036108.
[21] A. Fluerasu, M. Sutton, E. Dufresne, X-ray intensity fluctuation spectroscopy studies on phase-ordering systems, Phys. Rev. Lett. 94 (2005) 055501.
[22] L.M. Stadler, B. Sepiol, R. Weinkamer, M. Hartmann, P. Fratzl, J.W. Kantelhardt, F. Zontone, G. Grübel, G. Vogl, Long-term correlations distinguish coarsening mechanisms in alloys, Phys. Rev. B 68 (2003) 180101.
[23] L.M. Stadler, B. Sepiol, J.W. Kantelhardt, I. Zizak, G. Grübel, G. Vogl, Revealing antiphase-domain dynamics in alloys by combining advanced statistical techniques with x-ray photon correlation spectroscopy, Phys. Rev. B 69 (2004) 224301.
[24] I.K. Robinson, I.A. Vartanyants, G.J. Williams, M.A. Pfeifer, J.A. Pitney, Reconstruction of the shapes of gold nanocrystals using coherent x-ray diffraction, Phys. Rev. Lett. 87 (2001) 195505.
[25] J. Miao, D. Sayre, H.N. Chapman, Phase retrieval from the magnitude of the Fourier transforms of nonperiodic objects, J. Opt. Soc. Amer. A 15 (1998) 1662–1669.
[26] P. Thibault, M. Dierolf, O. Bunk, A. Menzel, F. Pfeiffer, Probe retrieval in ptychographic coherent diffractive imaging, Ultramicroscopy 109 (4) (2009) 338–343.
[27] H.N. Chapman, K.A. Nugent, Coherent lensless x-ray imaging, Nature Photon. 4 (2010) 833–839.
[28] V.L.R. Jacques, S. Ravy, D. Le Bolloc'h, E. Pinsolle, M. Sauvage-Simkin, F. Livet, Bulk dislocation core dissociation probed by coherent x rays in silicon, Phys. Rev. Lett. 106 (2011) 065502.
[29] I.K. Robinson, Y. Da, T. Spila, J.E. Greene, Coherent diffraction of individual dislocation strain fields, J. Phys. D: Appl. Phys. 38 (2005) A7–A10.
[30] M. Sutton, Y. Li, J.D. Brock, R.E. Thorne, X-ray intensity fluctuation spectroscopy measurements of the charge density wave of $NbSe_3$, J. Phys. IV France 12 (2002) 3–8.
[31] D. Le Bolloc'h, S. Ravy, J. Dumas, J. Marcus, F. Livet, C. Detlefs, F. Yakhou, L. Paolasini, Charge density wave dislocation as revealed by coherent x-ray diffraction, Phys. Rev. Lett. 95 (2005) 116401.
[32] D. Le Bolloc'h, V.L.R. Jacques, N. Kirova, J. Dumas, S. Ravy, J. Marcus, F. Livet, Observation of correlations up to the micrometer scale in sliding charge-density waves, Phys. Rev. Lett. 100 (9) (2008) 096403.
[33] V. Jacques, D. Le Bolloc'h, S. Ravy, C. Giles, F. Livet, S. Wilkins, Spin density wave dislocation in chromium probed by coherent x-ray diffraction, Eur. Phys. J. B 70 (2009) 317–325.
[34] R.T.T.I.K. Robinson, R. Feidenhans'l, X-ray interference method for studying interface structures, Phys. Rev. B 38 (1988) 3632–3635.
[35] F. Livet, G. Beutier, M. de Boissieu, S. Ravy, D. Le Bolloc'h, V. Jacques, Coherent scattering from silicon monocrystal surface, Surf. Sci. 605 (2011) 390–395.
[36] M.S. Pierce, K.C. Chang, D. Hennessy, V. Komanicky, M. Sprung, A. Sandy, H. You, Surface x-ray speckles: Coherent surface diffraction from Au(001), Phys. Rev. Lett. 103 (16) (2009) 165501.
[37] S.M. Gruner, Concepts and applications of Energy Recovery Linacs (ERLs), AIP Conf. Proc. 708 (2004) 153–156.
[38] S. Benson, M. Borland, D. Douglas, D. Dowell, C. Hernandez-Garcia, D. Kayran, G. Krafft, R. Legg, E. Moog, T. Obina, R. Rimmer, V. Yakimenko, X-ray sources by energy recovered linacs and their needed R&D, Nucl. Instr. Meth. A 637 (1) (2011) 1–11.